Chemical Communications

Dynamic Article Links ►

Cite this: DOI: 10.1039/c0xx00000x

www.rsc.org/xxxxxx

COMMUNICATION

Three Dimensional-TiO_2 nanotube array photoanode architectures assembled on thin hollow nanofibrous backbone and their performance in quantum dot-sensitized solar cells

Hyungkyu Han,[‡a] P. Sudhagar,[‡b,c] Taeseup Song,[a] Yeryung Jeon,[b] Iván Mora-Seró,[d] Francisco Fabregat-Santiago,[d] Juan Bisquert,[d] Yong Soo Kang[b,c*] and Ungyu Paik[a,b*]

Received (in XXX, XXX) Xth XXXXXXXXX 20XX, Accepted Xth XXXXXXXXX 20XX

DOI: 10.1039/b000000x

Facile synthesis of TiO_2 nanotube branched (length ~ 0.5 μm) thin hollow-nanofibers is reported. The hierarchical three dimensional photoanodes (H-TiO_2-NF) (only ~ 1 μm thick) demonstrate their excellent candidature as a photoanode in QDs-sensitized solar cells, exhibiting ~ 3 fold higher energy conversion efficiency (η =2.8%, J_{sc}=8.8 mAcm^{-2}) than that of the directly grown nanotube arrays on transparent conducting oxide (TCO) substrate (η =0.9%, J_{sc}=2.5 mAcm^{-2}) .

The mesoscopic sensitized-solar cell is the emerging candidate in electrical power production though direct conversion of solar energy to electrical energy without green house effect.[1] Recently, quantum dot (QDs) semiconductors have attracted a great deal of interest as sensitizers in mesoscopic sensitized solar cells.[2, 3] Because of the outstanding abilities in multiple hot carrier generation, panchromatic solar harnessing and high extinction coefficient, the quantum dot-sensitized solar cells (QDSCs) are being the future solar energy conversion systems.[4] Many efforts have been invested in developing a wide range of sensitizers; in particular, CdX, PbX, CuInX (X=S, Se, Te) and Ag_2S *etc.,* have been tested in QDSCs, resulting in ~ 4-6 % photo conversion efficiency.[5-7] These sensitizers are decorated on a wide band gap metal oxide framework (TiO_2, ZnO and SnO_2) that acts as a photoanode (selective electron contact). Though QDSCs demonstrate feasible performance utilizing a variety of QDs sensitizers, still it requires more improvement to compete with the commercial dye-sensitized solar cells.

Semiconductor QDs sensitizers are relatively larger in size than dye molecules; therefore it is difficult to penetrate deeper parts of TiO_2 electrode and thus limiting the sensitizer loadings. Although, the higher extinction coefficient of semiconductor QDs, in comparison with molecular dyes, partially compensates the loss of the effective surface and subsequently the decrease in the sensitizer loading, configuring the photoanode framework with large-pore network is necessary to further promote the QDs sensitizer loading.[8] In Addition, such photoanodes could demonstrate high charge transport from sensitizer to a charge collector, ultimately, overwhelming the charge recombination at photoanode/electrolyte interface. Thus, to achieve high sensitizer loading, fast electron transport channel, and good electrolyte pore-filling, establishing vertically aligned nanostructures, in particular, directly synthesized on transparent conductive oxides (TCO) has been identified as the promising approach in dye or QDs-sensitized solar cells.[9] Most importantly, vertically grown nanotube (NT) arrays have longer electron diffusion length and more benefits in pore-filling of solid state hole transport materials (HTM), compared to disordered TiO_2 mesoporous films.[10] Diverse methods were demonstrated for the fabrication of TiO_2 NT arrays, including electrochemical anodization,[11] hydrothermal treatment[12] and vapour-liquid-solid methods. Recently, *Gao* group developed directly assembled TiO_2 NT arrays on TCO using ZnO nanowire templates.[13] Though direct assembly of NT arrays on TCO substrates, is more adventurous,[14] template-based NT arrays have wide tube-tube voids which resulted in lesser distribution compared to anodization technique. Besides, such less density of NTs on a TCO substrate markedly lowers the internal surface area of the electrode as well as limits the QD loading.

One simple way to promote the interface surface area of the NT array is to extend their length,[15] however there exist a trade-off between the NT length and mechanical stability. Therefore, assembling NT array on highly interconnected 3D fibrous backbone would be a more effective way for achieving high electron transport channels in energy conversion devices.[16-18] Scheme 1 illustrates the fabrication stages of hierarchical 3-D hollow TiO_2 nanofibers (H-TiO_2-NF). Our proposed hierarchical 3-D hollow TiO_2 NFs would be the optimum nanostructure for achieving higher sensitizer loading and fast electron transport for QDSCs. In this communication, we demonstrate the fabrication of TiO_2 nanotubes branched on TiO_2 hollow nanofiber photoanode, directly grown on TCO and elucidate their candidature as an excellent photo anode in QDSCs.

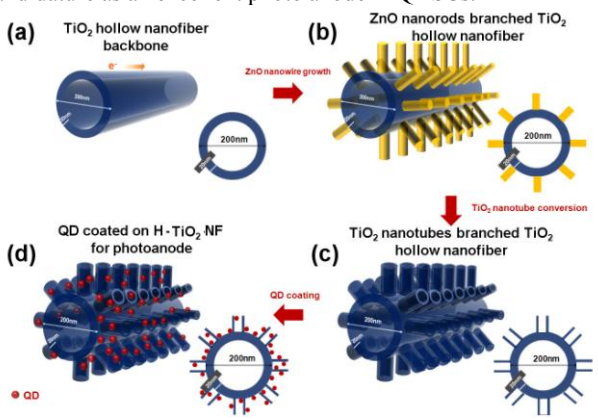

Scheme 1. Schematic illustration of H-TiO_2 NF photoanode fabrication stages (a) TiO_2 hollow nanofiber (TiO_2-NF), (b) ZnO NR templates grown on TiO_2-HNF, (c) TiO_2 nanotube branches grown on TiO_2-NF through ZnO NR templates, and (d) QDs-sensitized H-TiO_2 NF photoanode.

Figure 1 shows the scanning electron microscopy (SEM) image (Figure 1a) of backbone TiO_2 NFs confirming the continuous 1D geometry. The distribution of the fiber diameter lies between 200 and 500 nm with the average wall thickness of 20 nm. The ZnO NR templates with an average diameter ~ 25 nm and a length of ~500 nm were vertically grown on the outer surface of TiO_2 NF which completely covered the backbone (Fig. 1b). After the TiO_2 thin layer coating on ZnO NRs, the ZnO templates were finally removed by selective etching (Fig. 1c). Fig. 1d shows the QDs-sensitized 3-D TiO_2 nanotubes branched on TiO_2 hollow nanofibers (H-TiO_2 NF). The high resolution TEM images and the selective area electron diffraction pattern (SAED) reveal that the TiO_2 hollow nanofiber possess anatase phase and polycrystalline nature (Fig. 1e). Fig. 1(f) reveals that the spatially decorated ZnO NT arrays on TiO_2 NF have good contact with the TiO_2 backbone. Furthermore, TEM image (Fig. 2g and 2h) suggests that the TiO_2 tubular branches have sufficiently large pore channels for electrolyte filling as well as good structural stability even after removing the ZnO templates and QDs sensitization, respectively.

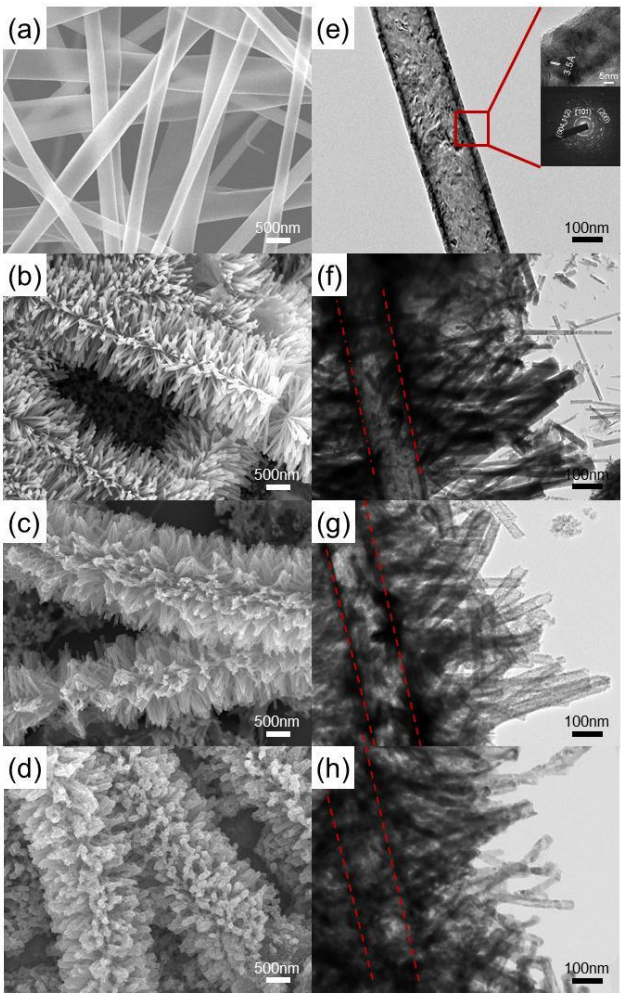

Figure 2. FE-SEM images (a-d) and HR-TEM images (e-h) of TiO_2 hollow nanofibers, ZnO nanorods branched on TiO_2 hollow nanofibers, TiO_2 nanotubes branched on TiO_2 hollow nanofibers, and QDs-sensitized 3-D TiO_2 nanotubes branched on TiO_2 hollow nanofibers respectively.

The detailed experimental procedure for the fabrication of hierarchical TiO_2 NFs and QDSCs device fabrication steps is explained in the supporting information **(see supporting information S1)**. To demonstrate the influence of electrode geometry on photovoltaic performance of QDSCs, the following electrodes were tested as photoanodes in QDSCs: (a) directly grown TiO_2 NT on TCO (TiO_2-NT) and (b) hierarchical 3-D TiO_2 nanotube branches on hollow TiO_2 NF (H-TiO_2 NF) electrodes. The optical reflection capability of both TiO_2-NT and H-TiO_2 NF is studied by diffused reflectance spectra (Fig. 2a). Under the identical TiO_2 nanotube growth conditions, the H-TiO_2 NF electrodes show high reflectance compared to TiO_2-NT in the wavelength range of 380-800nm. This might be attributed to the multiple scattering of incident light at the hierarchical TiO_2 NT branches, thus drastically enhancing the reflectance of the electrode. Both QDs-sensitized TiO_2-NT and H-TiO_2 NF electrodes found to be decreased in the reflectance at wavelength 610 and 660nm, respectively, due to the light absorption of the CdS/CdSe sensitizer. The photovoltaic performance (J-V plots) of TiO_2-NT and H-TiO_2 NF photoanodes were presented in Fig. 2b and the estimated PV parameters are summarized in Table 1.

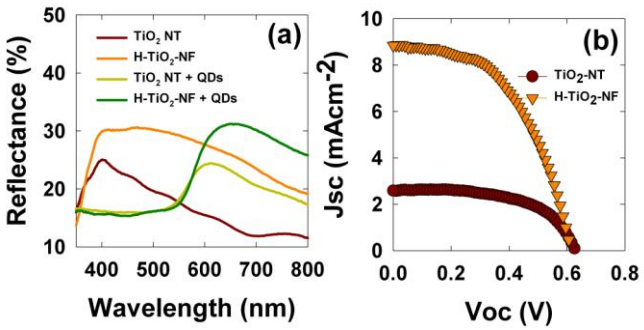

Figure 2. J-V plots of QDSCs using different photoanodes (Electrode thickness: ~ 1 μm, device active area: 0.25cm^{-2} without mask, electrolyte: 1M polysulfide and counter electrode: nanocarbon black).

The directly grown TiO_2-NTs on a FTO electrode resulted in a photoconversion efficiency (PCE) of c.a. η=0.9% with photovoltage, V_{oc}=0.62 V, photocurrent, J_{sc}=2.5 $mAcm^{-2}$ and fill factor, F.F=58.3%. As anticipated, the hierarchical TiO_2 nanotube branches grown on hollow NF backbone shows unprecedentedly promoted PCE to η=2.8% with V_{oc}=0.61 V, J_{sc}=8.8 $mAcm^{-2}$ and F.F.=50.3%. It clearly evidences that the TiO_2 NTs spatially assembled on the hierarchical 3D-nanofibrous backbone promote the QDSCs performance by a factor of three than the directly grown TiO_2 NTs on a TCO substrate. We can explain the enhancement of photocurrent generation with the H-TiO_2 NF photoanodes by several contributions: (a) higher effective surface area and consequently higher QD loading and light harvesting; (b) highly efficient charge collection throughout the photoanode with less boundary layers and (c) multiple scattering effect of the comb-like hierarchical NT arrays, in particular, red photons harvesting.

Table 1. Photovoltaic parameters of QDSCs using different photoanodes

Photo anode	V_{oc} *(V)*	J_{sc} *($mAcm^{-2}$)*	F.F. *(%)*	Efficiency *(%)*
TiO_2-NT	0.62	2.5	58.3	0.9
H-TiO_2 NF	0.61	8.8	50.3	2.8

On the other hand, it is interesting to point out that V_{oc} obtained for both devices are similar, in spite of the larger effective surface area of H-TiO_2 NF, expecting a higher recombination rate (and consequently lower V_{oc}). But this is not the case as observed in Fig. 2b, where similar V_{oc} values are observed for both the samples. For further understanding of this behaviour, the QDSCs recombination has been analyzed using the electrochemical impedance spectroscopy (EIS). The stability of the samples during the impedance measurement was verified by comparing the cyclic voltammograms before and after EIS measurement (**See supporting information S3**). Fig. 3 shows the recombination resistance obtained for the samples analyzed in Fig. 2b. Similar recombination resistances are observed for both samples. Despites the larger effective surface area of H-TiO_2 NFs, the recombination resistance does not become significantly higher than the resistance observed for TiO_2-NT.

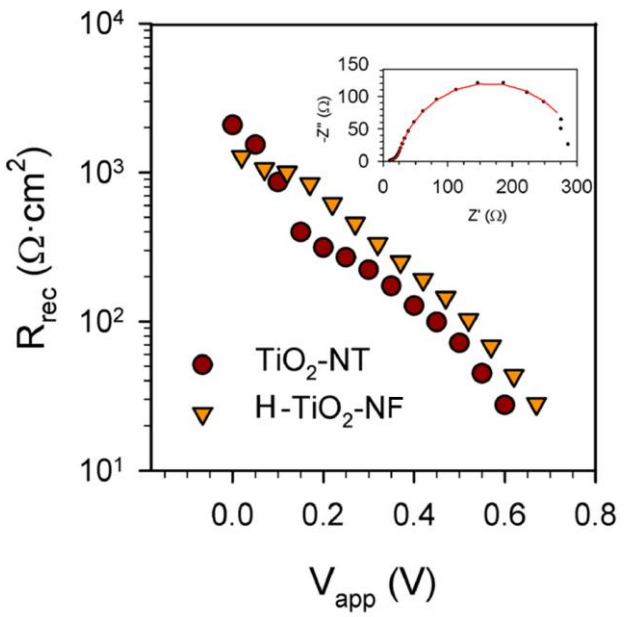

Figure 3. Recombination resistance of TiO_2-NT and H-TiO_2 NF QDSCs. Inset Nyquist plot of H-TiO_2 NF sample at applied voltage, V_{app}=0.57 V. Red solid line is the fit of the experimental data points using the previously described model for EIS analysis of QDSCs samples[7].

In this sense, the recombination rate does not increase for the hierarchical sample; rather it decreases as shown in Fig. 3. This fact may be contributable significantly to the 3 fold enhancement in the solar cell efficiency observed for the H-TiO_2 NFs in comparison with the TiO_2-NTs. The huge increase of photocurrent is not deleteriously compensated by a reduction in V_{oc}, giving place to a final efficiency improvement of 310%. In addition high collection efficiency can be deduced for H-TiO_2 NF QDSCs (**See supporting information S4**).

In summary, 3-D hierarchical TiO_2 nanotube branches were successfully assembled onto the primary hollow TiO_2 nanofibrous backbone. The newly designed H-TiO_2 NF photoanode has offered large surface area for high QD loading with high light scattering property. In comparison with the directly grown NT arrays on a TCO substrate, the introduction of NTs on the continuous hollow nanofibrous layer results in the effective charge collection. In addition, the hierarchical structure enhances effective surface area without altering the recombination rate, as it should be expected. The proposed H-TiO_2 NF architecture fabricated from the simple protocol can allow wide applications in electrochemical energy conversion and storage devices including QDSCs, DSSCs, photocatalyst and batteries, where high catalytic/electroactive materials have to be loaded and fast charge transport characteristics is required.

Acknowledgement

This work was supported by the Engineering Research Center Program through a National Research Foundation of Korea (NRF) grant funded by the Ministry of Education, Science and Technology (MEST) (No. 2012-0000591), World Class University (WCU) program (NoR31-2008-000-10092) and also by National Research Foundation of Korea (NRF) through Grant No. K20704000003TA050000310, Global Research Laboratory (GRL) Program provided by the Korean Ministry of Education, Science and Technology (MEST) in 2012.

Notes and references

[a] *Department of Materials Science & Engineering, and* [b] *World Class University Program Department of Energy Engineering and* [c] *Center for Next Generation Dye-Sensitized Solar Cells, Hanyang University, Seoul 133791, South Korea*
E-mail: upaik@hanyang.ac.kr (UP) and kangys@hanyang.ac.kr (YSK)
[d] *Photovoltaics and Optoelectronic Devices Group, Departament de Física Universitat Jaume I, 12071 Castelló, Spain*

† Electronic Supplementary Information (ESI) available: [Experimental and characterization details]. See DOI: 10.1039/b000000x/
‡ These authors contributed equally to the research.

1. A. Yella, H. W. Lee, H. N. Tsao, C. Y. Yi and A. K. Chandiran, *Science*, 2011, **334**, 1203-1203.
2. I. Mora-Sero and J. Bisquert, *J Phys Chem Lett*, 2010, **1**, 3046-3052.
3. P. V. Kamat, *J Phys Chem C*, 2008, **112**, 18737-18753.
4. S. Ruhle, M. Shalom and A. Zaban, *Chemphyschem*, 2010, **11**, 2290-2304.
5. A. Braga, S. Gimenez, I. Concina, A. Vomiero and I. Mora-Sero, *J Phys Chem Lett*, 2011, **2**, 454-460.
6. P. K. Santra and P. V. Kamat, *Journal of the American Chemical Society*, 2012, **134**, 2508-2511.
7. V. Gonzalez-Pedro, X. Q. Xu, I. Mora-Sero and J. Bisquert, *ACS nano*, 2010, **4**, 5783-5790.
8. M. Samadpour, S. Gimenez, P. P. Boix, Q. Shen, M. E. Calvo, N. Taghavinia, A. I. Zad, T. Toyoda, H. Miguez and I. Mora-Sero, *Electrochim Acta*, 2012, **75**, 139-147.
9. K. Zhu, N. R. Neale, A. Miedaner and A. J. Frank, *Nano letters*, 2007, **7**, 69-74.
10. J. Bandara, K. Shankar, J. Basham, H. Wietasch, M. Paulose, O. K. Varghese, C. A. Grimes and M. Thelakkat, *Eur Phys J-Appl Phys*, 2011, **53**.
11. J. Wang and Z. Q. Lin, *J Phys Chem C*, 2009, **113**, 4026-4030.
12. H. H. Ou and S. L. Lo, *Sep Purif Technol*, 2007, **58**, 179-191.
13. C. K. Xu, P. H. Shin, L. L. Cao, J. M. Wu and D. Gao, *Chem Mater*, 2010, **22**, 143-148.
14. P. Chen, J. Brillet, H. Bala, P. Wang, S. M. Zakeeruddin and M. Gratzel, *J Mater Chem*, 2009, **19**, 5325-5328.
15. C. K. Xu and D. Gao, *J Phys Chem C*, 2012, **116**, 7236-7241.
16. M. Shang, W. Z. Wang, W. Z. Yin, J. Ren, S. M. Sun and L. Zhang, *Chem-Eur J*, 2010, **16**, 11412-11419.
17. N. Tetreault, E. Horvath, T. Moehl, J. Brillet, R. Smajda, S. Bungener, N. Cai, P. Wang, S. M. Zakeeruddin, L. Forro, A. Magrez and M. Gratzel, *ACS nano*, 2010, **4**, 7644-7650.
18. P. Sudhagar, V. Gonzalez-Pedro, I. Mora-Sero, F. Fabregat-Santiago, J. Bisquert and Y. S. Kang, *J Mater Chem*, 2012, **22**, 14228-14235.